Supplementary Material for "GenBrain: A Generative Foundation Model of Multimodal Brain Imaging"

Chang Yang[1,2], Jianfeng Feng[1,2,3,4], Christian F. Beckmann[5,6,7], Stephen M. Smith[5], Weikang Gong[4,5,#]

1. Institute of Science and Technology for Brain-Inspired Intelligence, Fudan University, Shanghai, 200433, China.
2. Key Laboratory of Computational Neuroscience and Brain-Inspired Intelligence, Fudan University, Ministry of Education, Shanghai, 200433, China.
3. Department of Computer Science, University of Warwick, Coventry, United Kingdom.
4. School of Data Science, Fudan University, Shanghai, 200433, China.
5. Centre for Functional MRI of the Brain (FMRIB), Nuffield Department of Clinical Neurosciences, Oxford University Centre for Integrative Neuroimaging, University of Oxford, Oxford, OX3 9DU, UK.
6. Radboud University Medical Centre, Department of Cognitive Neuroscience, Nijmegen, Netherlands.
7. Donders Institute for Brain, Cognition and Behaviour, Radboud University Nijmegen, Nijmegen, Netherlands.

Corresponding author:
Weikang Gong, PhD. School of Data Science, Fudan University, Shanghai, 200433, China. E-mail address: weikanggong@fudan.edu.cn.

Contents

Supplementary Table 1 | Detailed information of 3D brain images across 34 modalities from the UK Biobank. This table provides detailed information including **modality name, index, and description**. Abbreviations: **DTI** (Diffusion Tensor Imaging), **NODDI** (Neurite Orientation Dispersion and Density Imaging), **rs-fMRI** (Resting-state functional MRI), and **FC** (functional connectivity).

Modality Name	Index	Description
DTI-FA	0	DTI-Fractional anisotropy
DTI-L1	1	DTI-Axial diffusivity
DTI-L2	2	DTI-Radial diffusivity
DTI-L3	3	DTI-Second radial diffusivity
DTI-MD	4	DTI-Mean diffusivity
DTI-MO	5	DTI-Mode of anisotropy
NODDI-ICVF	6	NODDI-Intracellular volume fraction
NODDI-ISOVF	7	NODDI-Isotropic volume fraction
NODDI-OD	8	NODDI-Orientation dispersion
QSM	9	Quantitative susceptibility mapping from SWI
SWI	10	Susceptibility-weighted imaging
T1w	11	T1-weighted MRI
T1-Jac	12	Jacobian map of T1w nonlinear registration
T2-FLAIR	13	T2-Fluid attenuated inversion recovery
T2star	14	T2* from SWI
VBM	15	Grey matter volume from voxel-based morphometry
Task-1	16	Task-based fMRI: Shapes contrast z-statistic maps
Task-2	17	Task-based fMRI: Faces contrast z-statistic maps
Task-5	18	Task-based fMRI: faces > shapes contrast z-statistic maps
Rest-1	19	rs-fMRI seed-based FC: Visual Peripheral
Rest-2	20	rs-fMRI seed-based FC: Cingulo-Opercular
Rest-3	21	rs-fMRI seed-based FC: Default Network-B
Rest-4	22	rs-fMRI seed-based FC: Somatomotor-B
Rest-5	23	rs-fMRI seed-based FC: Auditory
Rest-6	24	rs-fMRI seed-based FC: Premotor-Posterior Parietal Rostral
Rest-7	25	rs-fMRI seed-based FC: Dorsal Attention-B
Rest-8	26	rs-fMRI seed-based FC: Somatomotor-A
Rest-9	27	rs-fMRI seed-based FC: Language
Rest-10	28	rs-fMRI seed-based FC: Frontoparietal Network-B
Rest-11	29	rs-fMRI seed-based FC: Frontoparietal Network-A
Rest-12	30	rs-fMRI seed-based FC: Dorsal Attention-A
Rest-13	31	rs-fMRI seed-based FC: Visual Central
Rest-14	32	rs-fMRI seed-based FC: Salience / Parietal Memory Network
Rest-15	33	rs-fMRI seed-based FC: Default Network-A

Supplementary Table 2 | Information on datasets used in this study. Information about the number of sites (Site), subjects (Subject), scans (Scan), and image modality types (Modality) is provided. The UK Biobank dataset (used for pretraining and evaluation) contains 34 different image modalities; details are provided in Supplementary Table 1. For the ABIDE autism dataset, the Tian subcortical atlas was used to extract seed-based functional connectivity from the rs-fMRI data.

Dataset	Site	Subject	Number of Scan	Modality
UK Biobank (pretraining)	1	44,398	1,193,348	34 modalities
UK Biobank (evaluation)	1	2,000	68,000	34 modalities
ZIC Alzheimer's disease	1	1,138	2,271	T1w, T2-FLAIR
ADNI	1	768	2,632	T1w
Schizophrenia	17	2,958	5,780	T1w, VBM
ABIDE I and II (ASD)	36	1,778	1,778	rs-fMRI
Major Depressive Disorder (MDD)	24	2,831	2,831	VBM
SOOP (acute stroke)	1	1,106	1,106	DTI-ADC
ARC (chronic stroke)	1	213	213	DTI-FA

Supplementary Table 3 | Details information of multisite datasets in our study.

Information on the multisite datasets, including image modality (Modality), site name (Site), and number of subjects (Subjects), is provided.

Dataset	Modality	Site Name (Subjects)
Schizophrenia	T1w	HCP-EP (93), ds004302(66), CLB (90), NUSDAST (250), chengdu (228), taiwan (254), ds000115 (40), ds000030 (171), NMorphCH (87), SH_JZ1 (298), COBRE (165), MCIC (203), zhengzhou (253), SH_JZ2 (324), SH_ECT (65), SH_drug1 (255), fBIRN (107)
	VBM	HCP-EP (93), ds004302 (64), CLB (90), NUSDAST (250), chengdu (103), taiwan (254), ds000115 (40), ds000030 (171), NMorphCH (87), SH_JZ1 (298), COBRE (165), MCIC (204), zhengzhou (253), SH_JZ2 (330), SH_ECT (65), SH_drug1 (257), fBIRN (107)
ABIDE I and II (ASD)	rs-fMRI	STANFORD (36), ABIDEII-GU_1 (99), ABIDEII-NYU_2 (27), ABIDEII-BNI_1 (54), ABIDEII-SDSU_1 (55), ABIDEII-OHSU_1 (86), YALE (48), CMU (5), ABIDEII-NYU_1 (72), NYU (171), LEUVEN_2 (32), OHSU (23), ABIDEII-EMC_1 (54), UM_2 (31), USM (61), ABIDEII-ETH_1 (34), ABIDEII-KKI_1 (198), SBL (26), ABIDEII-OILH_2 (58), UM_1 (82), ABIDEII-IU_1 (36), ABIDEII-KUL_3 (28), UCLA_1 (55), OLIN (25), PITT (45), TRINITY (44), MAX_MUN (42), ABIDEII-UCD_1 (13), LEUVEN_1 (29), UCLA_2 (20), ABIDEII-IP_1 (51), ABIDEII-TCD_1 (21), SDSU (33), KKI (39), ABIDEII-UCLA_1 (8), CALTECH (37)
Major Depressive Disorder	VBM	S1 (148), S2 (60), S3 (64), S5 (24), S6 (30), S7 (87), S8 (150), S9 (100), S10 (83), S11 (61), S12 (38), S13 (42), S14 (96), S15 (100), S16 (62), S17 (91), S18 (41), S19 (87), S20 (533), S21 (156), S22 (50), S23 (62), S24 (63), S25 (152)

Supplementary Table 4 | Raw BWAS performance metrics corresponding to Fig. 5. Raw quantitative metrics underlying the relative improvements reported in Fig. 5, comparing real and synthetic data for brain-wide association studies (BWAS) across Schizophrenia (SCZ), Major Depressive Disorder (MDD), and Autism Spectrum Disorder (ASD). Metrics include Pearson correlation between voxel-wise Cohen's *d* maps, Dice coefficients computed on the full map and on positive ($d > 0$) and negative ($d < 0$) effects, as well as Dice coefficients restricted to the top 20% of absolute Cohen's *d* values. Relative improvements shown in Fig. 5 were computed from these raw values.

Site	Disease	Data	Correlation	Dice	Dice-p	Dice-n	top-Dice	top-Dice-p	top-Dice-n
SH_JZ2	SCZ	Real	0.17	0.59	0.35	0.65	0.19	0.05	0.20
SH_JZ2	SCZ	Syn.	0.29	0.69	0.37	0.77	0.29	0.08	0.30
SH_JZ1	SCZ	Real	0.27	0.64	0.38	0.72	0.25	0.12	0.26
SH_JZ1	SCZ	Syn.	0.30	0.68	0.38	0.76	0.27	0.18	0.28
S20	MDD	Real	0.13	0.65	0.34	0.74	0.19	0.03	0.21
S20	MDD	Syn.	0.18	0.67	0.37	0.76	0.19	0.06	0.21
S9	MDD	Real	0.01	0.65	0.34	0.74	0.11	0.03	0.12
S9	MDD	Syn.	0.01	0.67	0.37	0.76	0.16	0.04	0.17
NYU	ASD	Real	0.21	0.57	0.62	0.48	0.10	0.11	0.09
NYU	ASD	Syn.	0.27	0.60	0.67	0.48	0.31	0.35	0.09
KKI_1	ASD	Real	0.16	0.68	0.77	0.32	0.23	0.24	0.01
KKI_1	ASD	Syn.	0.22	0.71	0.81	0.34	0.25	0.25	0.03

Supplementary Table 5 | Selected brain regions segmented using WMH-SynthSeg. Region names and labels are listed, and their volumes were computed as features for the LightGBM classification task.

Region	Label	Regions	Label
Left cerebral white matter	2	Left cerebral cortex	3
Left lateral ventricle	4	Left cerebellum white matter	7
Left cerebellum cortex	8	Left thalamus	10
Left caudate	11	Left putamen	12
Left pallidum	13	3rd ventricle	14
4th ventricle	15	Brainstem	16
Left hippocampus	17	Left amygdala	18
Extracerebral CSF	24	Left accumbens	26
Left ventral DC	28	Right white matter	41
Right cortex	42	Right lateral ventricle	43
Right cerebellum white matter	46	Right cerebellum cortex	47
Right thalamus	49	Right caudate	50
Right putamen	51	Right pallidum	52
Right hippocampus	53	Right amygdala	54
Right accumbens	58	Right ventral DC	60
WMH	77	Optic chiasm	85

Supplementary Table 6 | Hyperparameter settings of LightGBM. For data augmentation in machine learning–based disease diagnosis, the classification experiment was repeated 20 times for each synthetic-to-real ratio using randomly selected combinations of LightGBM hyperparameters.

Hyperparameter	Value	Description
n_estimators	{25,50,100,200,300}	Number of boosted trees to fit.
max_depth	{5, 10, 15, 20, 25, 30}	Maximum tree depth for base learners.
num_leaves	{5, 10, 15, 20, 25, 30}	Maximum number of leaves in one tree.
subsample	{0.60, 0.65, 0.70, …, 1.00}	Subsample ratio of the training instance.
learning_rate	{0.1, 0.05, 0.01, 0.001}	Learning rate.
colsample_bytree	{0.60, 0.65, 0.70, …, 1.00}	Subsample ratio of columns when constructing each tree.
boosting_type	{‘gbdt’}	Traditional gradient boosting decision tree.

Supplementary Note 1 | Extending GenBrain to other non-imaging variables

GenBrain was originally pretrained on the UK Biobank (UKB) dataset, using subject-specific biological variables—age and sex—as conditions for image generation. To examine whether GenBrain could also model images conditioned on other non-imaging phenotypic variables, we introduced fluid intelligence scores as an additional condition and fine-tuned the model on a subset of 1,000 subjects (26,939 images) from the UKB pretraining data. Fine-tuning was performed for 50,000 steps with a batch size of 64.

To evaluate the extent to which fluid intelligence–related patterns were preserved in the generated images, we followed the same procedure used to assess age- and sex-related biological patterns. Population-level pseudo–ground truth maps for fluid intelligence were constructed as voxel-wise t-statistic maps derived from a reference cohort (N = 18,345), with missing values imputed using the mean score (6.576).

Even when fine-tuned on only 1,000 subjects, GenBrain successfully captured fluid intelligence–associated spatial patterns in both structural MRI and task fMRI images. Quantitative evaluation results are provided in Supplementary Fig. 1.

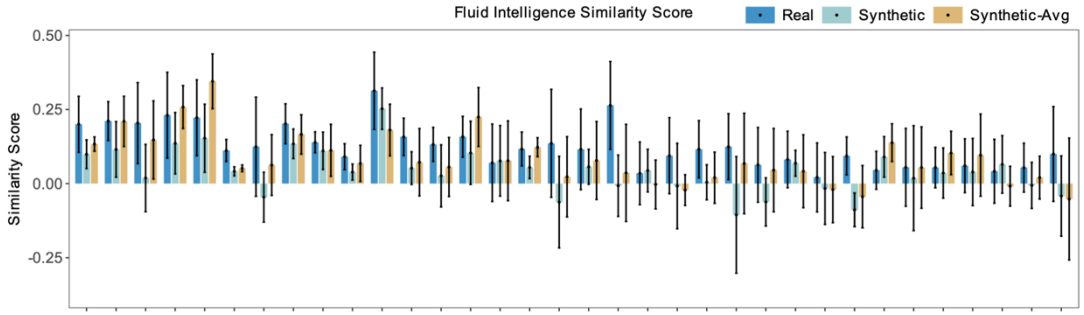

Supplementary Fig. 1 | Preservation of fluid intelligence–related patterns in synthetic images. GenBrain was fine-tuned on 1,000 subjects and extended to incorporate fluid intelligence scores as a new non-imaging conditional variable. The fluid intelligence–related pattern was evaluated on randomly sampled small cohorts (N = 100) of real data, synthetic data, and synthetic data averaged from five samples. The similarity score, defined as the cosine similarity between each small cohort's voxel-wise t-statistic map and that of the large reference cohort (N = 18,345), quantifies pattern preservation (higher scores indicate better preservation).

Supplementary Note 2 | Image enhancement-SynthSR pipeline

SynthSR[1,2] is a tool that can standardize clinical brain scans into high-resolution, isotropic 1 mm T1w images and enhance low-field images with limited resolution and signal-to-noise ratios by using "--lowfield" option[3]. In the image enhancement task, we applied SynthSR to enhance the corrupted T1w image. The image processing pipeline consisted of three steps. First, SynthSR was used to super-resolve and synthesize 1 mm T1w images with the skull retained. The command used was:

```
mri_synthsr --i {corrupted_image} --o {image_with_skull} --threads {threads} --lowfield
```

Second, the skull was removed using FreeSurfer SynthStrip[4]. The command used was:

```
mri_synthstrip --i {image_with_skull} --o {brain_image} --threads {threads}
```

Finally, the skull-stripped images were registered to MNI152 2 mm standard space using FreeSurfer SynthMorph[5]. The command used was:

```
mri_synthmorph register -o {registered_image} -j {threads} -g {brain_image} {mni152_2mm}
```

In the above commands, all variables enclosed in curly brackets "{}", except for "`threads`", represent data paths. The "`registered_image`" denotes the final enhanced image. The number of processing threads in our experiment was set to 16. We also applied this pipeline by replacing "`corrupted_image`" with "`flair_image`" for the FLAIR-to-T1w cross-modality synthesis experiment.

Supplementary Note 3 | White matter hyperintensities analysis

In clinical practice, T2-FLAIR images are pivotal for detecting white matter hyperintensities (WMH), a neuroimaging biomarker widely associated with cognitive decline and an increased risk of Alzheimer's disease. Beyond achieving high performance on image-level and biological semantic-level metrics, high-fidelity synthetic T2-FLAIR images should also preserve clinically meaningful features such as WMH to ensure translational utility. To this end, we employed WMH-SynthSeg[6] to automatically segment and estimate the volume of WMH in the synthesized T2-FLAIR images (WMH label: 77).

For the cross-modality synthesis task, we performed WMH analysis on synthetic FLAIR images generated in the T1w-to-FLAIR task. WMH were first segmented, and their volumes were estimated in both real images and synthetic images generated by different methods. We then computed the correlation of WMH volumes between paired real and synthetic images to evaluate how well the synthetic images preserved WMH features.

In the inner-dataset evaluation, GenBrain-ft achieved the highest correlation score (0.928) on the UKB dataset (N = 500). In the external evaluation on the ZIC dataset (N = 200), TUMSyn and GenBrain-ft obtained similar best correlation scores (TUMSyn: 0.922; GenBrain-ft: 0.911). The strong generalization performance of TUMSyn can be attributed to its multi-dataset training strategy, whereas GenBrain-ft benefited from generative pretraining on the UKB dataset. Detailed results are provided in Supplementary Fig. 2.

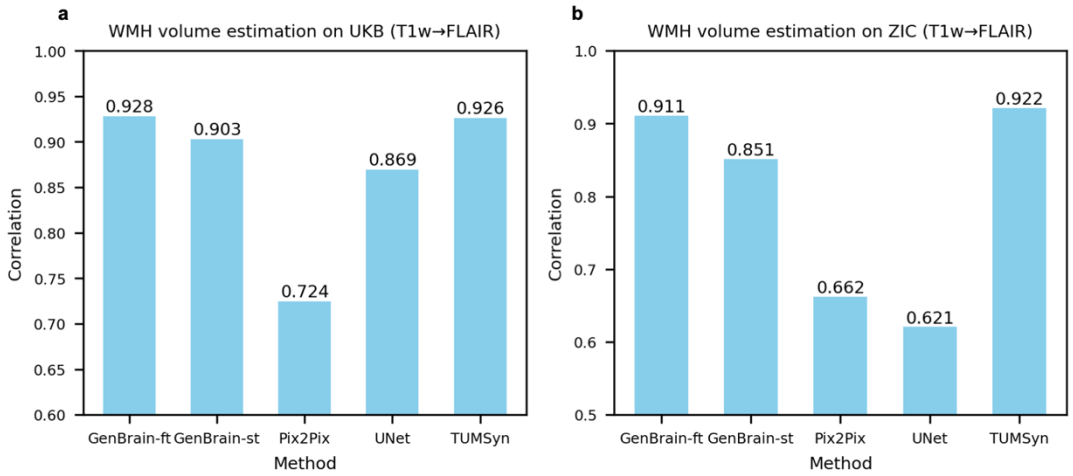

Supplementary Fig. 2 | Correlation of WMH volumes between paired real and synthetic images. WMH analysis was performed on synthetic FLAIR images in the T1w-to-FLAIR experiments. Internal dataset evaluation was conducted on the UKB dataset, and external evaluation on the ZIC dataset. High correlation indicates that the synthetic images reliably reproduce the WMH volume patterns existed in real T1w images.

Supplementary Note 4 | Fine-tuning GenBrain for image super-resolution

GenBrain was originally pretrained and analyzed in the MNI152 2 mm standard space (voxel size: $2 \times 2 \times 2\ mm^3$). To evaluate its adaptability to higher-resolution images, we fine-tuned the model to perform super-resolution from MNI152 2 mm to MNI152 1 mm standard space.

To adapt GenBrain for super-resolution, low-resolution (2 mm) T1-weighted images were first upsampled to 1 mm resolution using nearest-neighbor interpolation. Because directly applying the model's patch embedding to high-resolution images would incur a quadratic increase in computational cost due to the self-attention mechanism, we divided the interpolated images into eight equal-sized parts. Each part contained 228,453 voxels, the same number as in the corresponding low-resolution input, and was assigned a unique part index. The original single-channel patch embedding layer was replaced with a two-channel embedding layer, and a new image part–index embedder was introduced. This fine-tuned model is denoted as GenBrain-SR.

During fine-tuning, each interpolated part was concatenated with its corresponding noised high-resolution image part along the channel dimension to form a two-channel input tensor. GenBrain-SR was conditioned on this input tensor, the modality, and the part indices; age and sex embeddings were omitted. Fine-tuning was performed for 50,000 steps with a batch size of 64, using 1,000 paired T1w images (at both MNI152 1 mm and 2 mm resolutions) from the UK Biobank pretraining dataset.

During inference, GenBrain-SR generated high-resolution outputs part-by-part. These parts were subsequently combined into a complete high-resolution image by averaging the values of overlapping voxels. We found that GenBrain-SR could not only super-resolve real images but also further enhance synthetic images, such as the 2 mm T1w images initially generated by GenBrain-ft. Representative examples are provided in Supplementary Fig. 3.

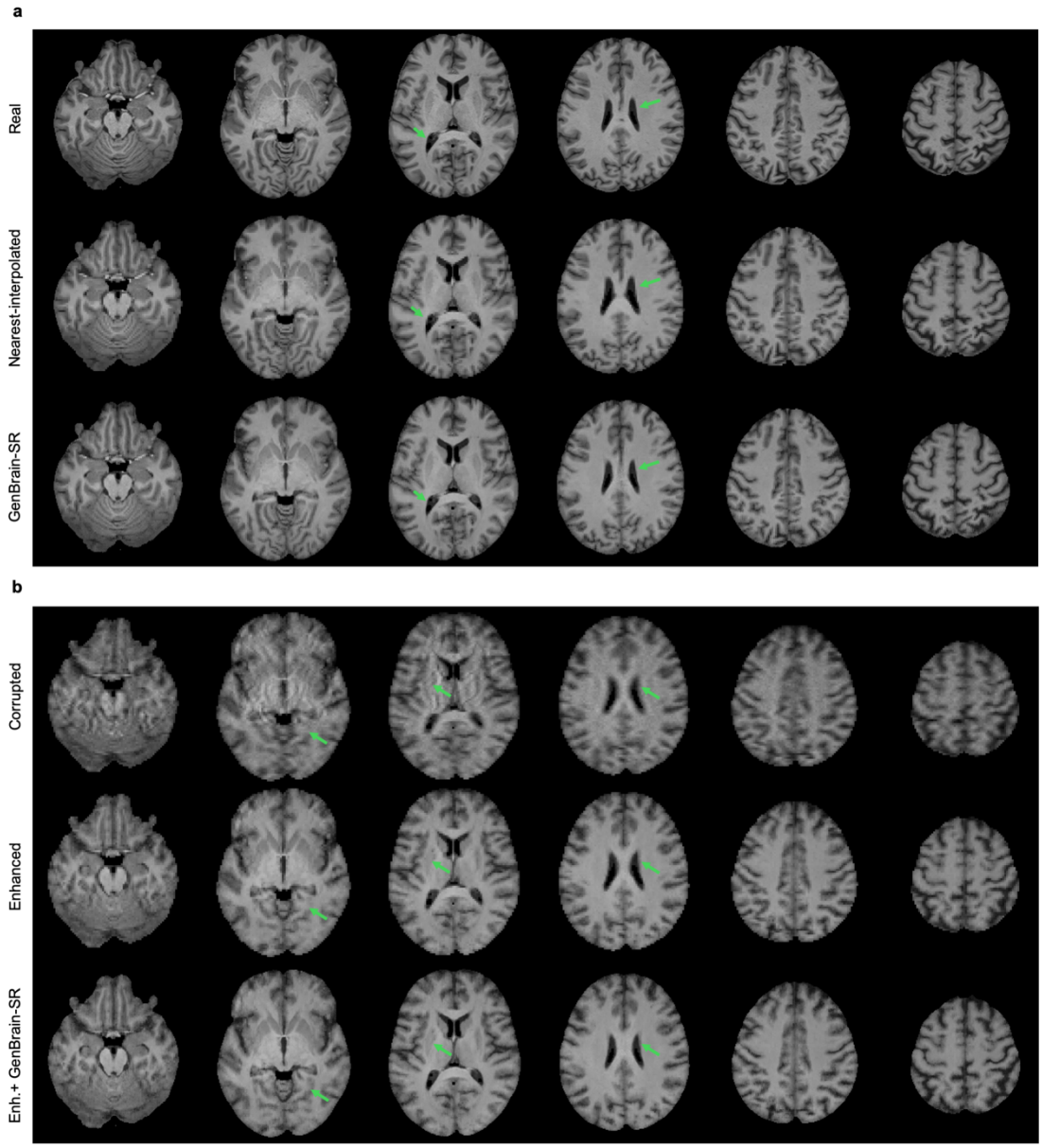

Supplementary Fig. 3 | Fine-tuning GenBrain for image super-resolution (MNI152 2 mm → 1 mm). a, Examples of high-resolution T1w images (1 mm), nearest-neighbor–interpolated T1w images (2mm → 1mm), and GenBrain-SR processed T1w images. **b,** Examples of corrupted T1w images (2 mm), GenBrain-ft–enhanced T1w images (2 mm), and the enhanced T1w images further super-resolved by GenBrain-SR (1 mm).

Supplementary Note 5 | Fine-tuning GenBrain for cross-modality synthesis (MNI152 1 mm standard space).

To further evaluate GenBrain's adaptability to higher-resolution images, we conducted T1w to T2-FLAIR and T2-FLAIR to T1w cross-modality synthesis tasks with images registered in MNI152 1mm standard space. Similar to the image super-resolution task, each source modality image was divided into eight parts of equal size, and GenBrain adopted the same architectural modifications, including a two-channel patch embedding layer and an image part–index embedder. GenBrain was conditioned on the source image, target modality and part indices, while age and sex embeddings were removed. GenBrain was fine-tuned for 50,000 steps with a batch size of 64 using 1,000 paired images (source–target modality pairs) from the UK Biobank pretraining dataset. At inference, the model translated the source images part-wisely, and then combined image parts into the target modality images (overlapped voxels using the average value). Cross-modality synthesis results see Supplementary Fig. 4.

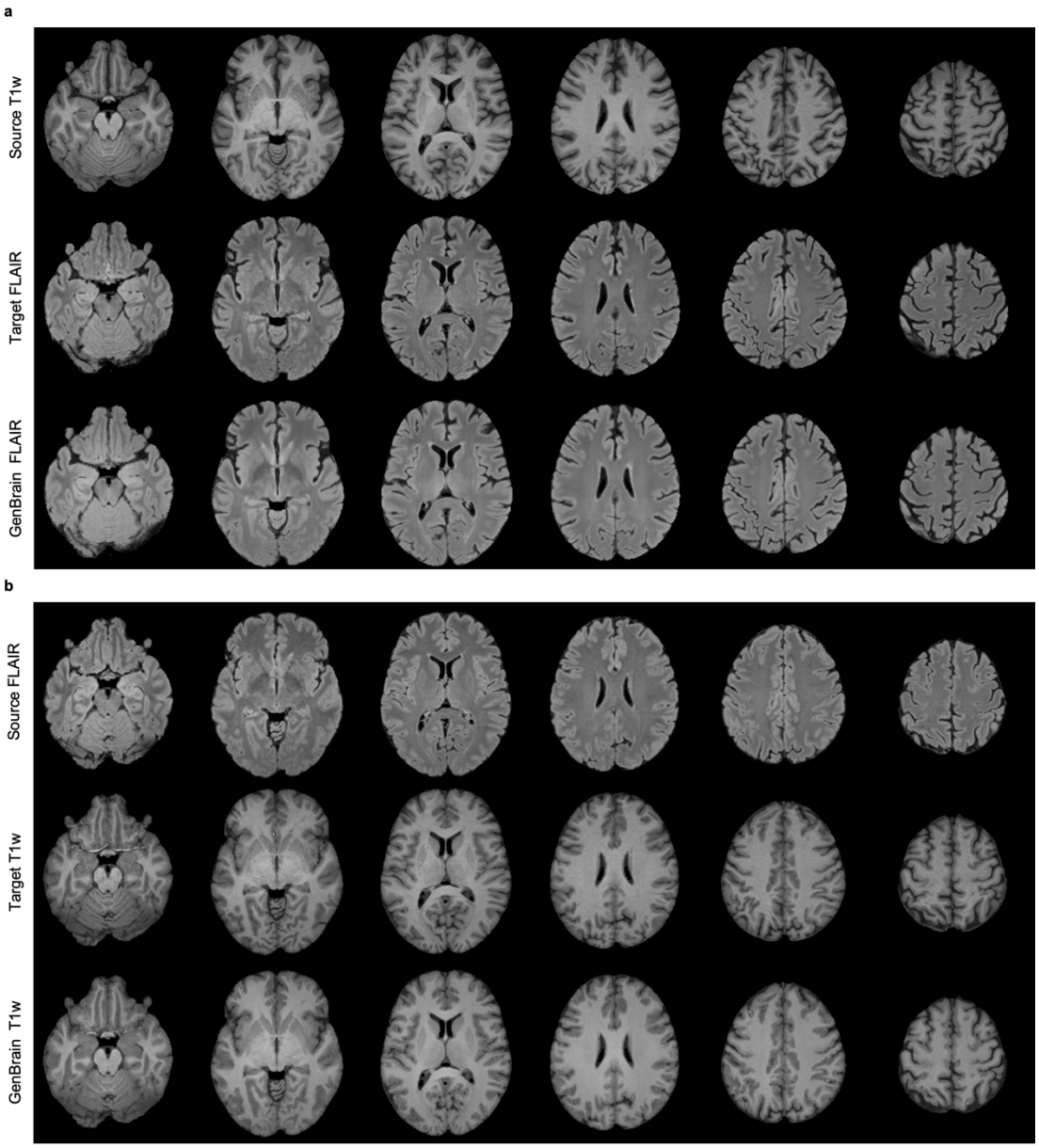

Supplementary Fig. 4 | Fine-tuning GenBrain for cross-modality synthesis (MNI152 1 mm). a, T1w to T2-FLAIR synthesis. Examples of source T1w images, target T2-FLAIR images, and GenBrain synthesized T2-FLAIR images are shown. **b**, T2-FLAIR to T1w synthesis. Examples of source T2-FLAIR images, target T1w images, and GenBrain synthesized T1w images are shown.

References

1. Iglesias, J.E.*, et al.* Joint super-resolution and synthesis of 1 mm isotropic MP-RAGE volumes from clinical MRI exams with scans of different orientation, resolution and contrast. *Neuroimage* **237**, 118206 (2021).
2. Iglesias, J.E.*, et al.* SynthSR: A public AI tool to turn heterogeneous clinical brain scans into high-resolution T1-weighted images for 3D morphometry. *Science advances* **9**, eadd3607 (2023).
3. Iglesias, J.E.*, et al.* Quantitative brain morphometry of portable low-field-strength MRI using super-resolution machine learning. *Radiology* **306**, e220522 (2022).
4. Hoopes, A., Mora, J.S., Dalca, A.V., Fischl, B. & Hoffmann, M. SynthStrip: skull-stripping for any brain image. *NeuroImage* **260**, 119474 (2022).
5. Hoffmann, M.*, et al.* SynthMorph: learning contrast-invariant registration without acquired images. *IEEE transactions on medical imaging* **41**, 543–558 (2021).
6. Laso, P.*, et al.* Quantifying white matter hyperintensity and brain volumes in heterogeneous clinical and low-field portable MRI. in *2024 IEEE International Symposium on Biomedical Imaging (ISBI)* 1–5 (IEEE, 2024).